

## **Dynamic Analysis of a Layered Cylinder Reinforced by Functionally Graded Carbon Nanotubes Distributions Subjected to Shock Loading using MLPG Method**

**Soleiman Ghouhestani<sup>1</sup>, Farzad Shahabian<sup>1</sup> and Seyed Mahmoud Hosseini<sup>2,3</sup>**

**Abstract:** In this paper, the meshless local Petrov-Galerkin (MLPG) method is exploited for dynamic analysis of functionally graded nanocomposite cylindrical layered structure reinforced by carbon nanotube subjected to mechanical shock loading. The carbon nanotubes (CNTs) are distributed across radial direction on thickness of cylinder, which can be simulated by linear and nonlinear volume fraction. Free vibration and elastic wave propagation are studied for various value of volume fraction exponent at various time intervals. The layered cylinder is assumed to be under axisymmetric and plane strain conditions. Four types of CNTs distributions including uniform and three kinds of functionally graded distributions along the radial of cylinder are considered. Material properties are simulated by a micro mechanical model. In the MLPG analysis, radial basis function (RBF) is used for approximation of displacement field in the weak form of governing equations and Heaviside function is used as test Function. For time domain analysis, the Newmark finite difference method is used. Effects of various distributions of carbon nanotubes on the propagation of elastic wave are illustrated and studied in details. The results obtained by the present analysis are compared and validated with those obtained by FEM, which were reported in previous published literatures.

**Keywords:** Meshless local Petrov-Galerkin method, Cylindrical layered structure, Dynamic analysis, Radial basis function, Carbon nanotubes, Nanocomposite.

---

<sup>1</sup> Civil Engineering Department, Faculty of Engineering, Ferdowsi University of Mashhad, Mashhad, Iran.

<sup>2</sup> Industrial Engineering Department, Faculty of Engineering, Ferdowsi University of Mashhad, Mashhad, Iran.

<sup>3</sup> Corresponding author. Tel: +98 511 8805064; Fax: +98 511 8763301;  
E-mails: sm\_hosseini@um.ac.ir; sm\_hoseini@yahoo.com

## 1 Introduction

The dynamic analysis of reinforced cylinder has received widespread attention in engineering applications. There are some literatures in which the layered structures were analyzed by numerical methods such as FEM and other well-known numerical methods [Dong (1968); Bert, Baker and Egle (1969); Stavsky and Loewy (1971); Greenberg and Stavsky (1980); Yamada, Irie and Tsushima (1984)]. Also, the dynamic analysis of FG structures has been studied using some mesh based numerical methods [Shahsiah and Eslami (2003); Fukui and Yamanaka (1992); Zimmerman and Lutz (1999); El-abbasi and Meguid (2000); Jabbari, Sohrabpour and Eslami (2002); Praveen and Reddy (1998); Awaji (2001); Loy, Lam and Reddy (1999)].

In the recent years, meshless method has found attentions in engineering problems. One of the very well-known meshless method is meshless local Petrov-Galerkin (MLPG) method, which has acceptable accuracy in the most engineering problems. In meshless methods, some nodes are distributed on analyzed domain with regular or random distributions, which nodes don't need to connect into elements. Thus, some difficulties associated with element based method may be overcome.

The MLPG concept was firstly presented by Atluri and Zhu [Atluri and Zhu (1998)]. Sladek et al. [Sladek, Sladek and Zhang (2003)] developed the MLPG method to solve transient elastodynamic initial-boundary value problem in continuously non-homogeneous solids. In their problem, the governing equations were transferred to frequency domain by Laplace transformation and local boundary integral equations were calculated and approximated in Laplace domain. Application of MLPG method in electromagnetic using radial basis functions was studied by Benbouza et al. [Benbouza, Louai and Nait-Said (2008)]. They used radial basis functions (RBFs) for interpolation of trial functions instead of the traditional moving least square (MLS) interpolations.

Gu et al. [Gu and Liu (2001)] used MLPG method for free and forced vibration analyses of solids. Local weak forms were developed using weighted residual method locally from the dynamic partial differential equations, in their research. In the free vibration analysis, the essential boundary conditions were implemented through the direct interpolation form and imposed using orthogonal transformation techniques. In the forced vibration analysis, the penalty method was used in implementation essential boundary conditions.

A comparison study of the efficiency and accuracy of a variety of meshless trial and test functions were studied by Atluri and Shen [Atluri and Shen (2002)], based on the general concept of the MLPG method. They used 5 types of trial functions and 6 types of test functions, in their work. It was shown that all of the MLPG methods possess excellent rates of convergence, for both the unknown variables and their

derivatives.

Two MLPG formulations based on Heaviside step functions and Gaussian weight functions were presented to analyze the dynamic behavior of elastic and elastoplastic solids by Soares Jr. et al. [Soares, Sladek and Sladek (2009)]. For both formulations, a MLS interpolation scheme was adopted, considering time-domain system of second order ordinary differential equations. In another research, they used their presented method for nonlinear analysis of the dynamic behavior of elastic and elastoplastic solids [Soares, Sladek and Sladek (2010)]. The propagation of thermoelastic waves in a FG thick hollow cylinder and coupled thermoelasticity analysis considering without and with Gaussian uncertainty in mechanical properties were studied by Hosseini et al. [Hosseini, Shahabian, Sladek and Sladek (2011); Hosseini, Sladek and Sladek (2011)] using MLPG method.

Reinforcing of structures especially layered cylinders is an important issue in engineering applications. Recently, the layered structures are reinforced by uniform or linear distribution of carbon nanotubes (CNTs) through a certain direction (radial and axial direction in cylinders).

Han and Elliott [Han and Elliott (2007)] studied the application of CNTs in the longitudinal direction to increase some mechanical properties in reinforced polymer matrix using constant strain energy minimization method. Coto et al. [Coto, Antia, Blanco, Martinez-de-Arenaza, Meaurio, Barriga and Sarasua (2011)] employed molecular dynamic method to show the effect of carboxylic groups attached on the surface of single wall carbon nanotube and multiwall carbon nanotube on their Young's modulus and Poisson's ratio along the axial direction of the CNTs. The mechanical properties of polymeric composites can be improved by using the single wall carbon nanotube reinforced matrix [Zhu, Pan and Roy (2007)].

The CNTs can be distributed as some grading patterns through a certain direction to improve the mechanical properties and to reinforce the composite structures. The composites, which are reinforced by CNTs with grading distribution, are called functionally garded nanocomposites reinforced by CNTs.

Recently, a meshless method was developed by Moradi-dastjerdi et al. [Moradi-Dastjerdi, Foroutan and Pourasghar (2013)] for dynamic analysis of nanocomposite cylinders with infinite length reinforced by single-walled carbon nanotubes subjected to a mechanical loading. Buckling analysis of functionally graded carbon nanotube reinforced composite plates using the element-free kp-Ritz method was studied by Lei et al. [Lei, Liew and Yu (2013a)]. In their work, the first-order shear deformation plate theory was applied and a set of meshless kernel particle functions was used to approximate two-dimensional displacement fields. They concluded that the change of carbon nanotube volume fraction, width-to-thickness ratio of

plate, plate aspect ratio, loading condition and temperature have significant effects on buckling strength of carbon nanotubes reinforced composite as well as the boundary conditions. In another research, they [Lei, Liew and Yu (2013b)] explored large deflection analysis of functionally graded carbon nanotube-reinforced composite plates by the element-free kp-Ritz method. The nonlinear governing equations were developed to investigate problems related to small strains and moderate rotations, based on the first-order shear deformation plate theory and von Kármán strains. Hosseini [Hosseini (2013)] used a hybrid meshless method for natural frequency analysis. Elastic wave propagation in a functionally graded nanocomposite reinforced by carbon nanotubes employing meshless local integral equation was studied by Ghayumizadeh et al. [Ghayumizadeh, Shahabian and Hosseini (2013)]. In this paper, a meshless method based on the local Petrov–Galerkin is developed to study elastic wave propagation and dynamic analysis in a layered nanocomposite cylinder reinforced by carbon nanotubes with infinite length. Numerical results for shock loading are presented to illustrate the applicability of the proposed method. The propagation of displacement waves are obtained at various time instants. Effects of some parameters such as grading pattern of carbon nanotubes distributions; orientation of ply in CNTs on dynamic analysis and wave propagation are investigated.

## 2 Reinforced functionally graded nanocomposites

Functionally graded materials are special composites in which volume fraction of constituent materials varies uniformly and continuously along a certain direction(s). Therefore, this kind of materials has a non-uniform microstructure and a continuously variable macrostructure by using this concept.

Shen [Shen (2009); Shen (2011)] suggested that the interfacial bonding strength can be improved by using a graded distribution of CNTs in the matrix. In this study, the influence of four type of CNTs distribution on wave propagation in a layered cylinder reinforced by CNTs; has been evaluated. The effective mechanical properties of such a cylinder can be obtained based on a micromechanical model as follows [Shen (2009)]:

$$E_1 = \eta_1 V_{CN} E_1^{CN} + V_m E^m, \quad (1)$$

$$\frac{\eta_2}{E_2} = \frac{V_{CN}}{E_2^{CN}} + \frac{V_m}{E^m}, \quad (2)$$

$$\frac{\eta_3}{G_{12}} = \frac{V_{CN}}{G_{12}^{CN}} + \frac{V_m}{G^m} \quad (3)$$

$$v_{ij} = V_{CN} v_{ij}^{CN} + V_m v^m, \quad i, j = 1, 2, 3 \quad i \neq j, \quad (4)$$

$$\rho = V_{CN}\rho^{CN} + V_m\rho^m, \quad V_{CN} + V_m = 1, \tag{5}$$

where  $E_1^{CN}, E_2^{CN}, G_{12}^{CN}, \nu^{CN}$  and  $\rho^{CN}$  are elasticity modulus, shear modulus, Poisson's ratio and density of the carbon nanotube, respectively, and  $E^m, G^m, \nu^m, \rho^m$  are corresponding properties for the matrix. The terms  $V_{CN}$  and  $V_m$  are volume fractions of carbon nanotube and matrix, respectively. The subscripts CN and m stands for carbon nanotube and matrix.  $\eta_J (J = 1, 2, 3)$  are CNTs efficiency parameters. Four kinds of distribution of CNT along the radial direction in a FGCNTs layered cylinder are presented as follows:

$$V_{CN} = V_{CN}^*, \quad \text{type UD} \tag{6}$$

$$V_{CN} = 2 \left( \frac{r_0 - r}{r_0 - r_i} \right) V_{CN}^*, \quad \text{type V} \tag{7}$$

$$V_{CN} = 4 \left| \frac{r - r_m}{r_0 - r_i} \right| V_{CN}^*, \quad r_m = \frac{r_i + r_0}{2}, \quad \text{type X} \tag{8}$$

$$V_{CN} = 2 \left( \frac{r - r_i}{r_0 - r_i} \right) V_{CN}^*, \quad \text{type } \Lambda \tag{9}$$

where

$$V_{CN}^* = \frac{\rho^m}{w^{CN} + \left( \frac{\rho^{CN}}{w^{CN}} \right) - \rho^{CN}}, \tag{10}$$

The term  $w^{CN}$  is the mass fraction of nanotube.

### 3 Mathematical formulations

According to a mechanical solid concept, the cylinder equilibrium equations in a domain  $\Omega$ , which is bounded by  $\Gamma$ , are presented by:

$$\sigma_{rr,r} + \tau_{rz,z} + \frac{1}{r} (\sigma_{rr} - \sigma_{\theta\theta}) + b_r = \rho(r, z) \ddot{u}_r, \tag{11}$$

$$\tau_{rz,r} + \sigma_{zz,z} + \frac{1}{r} \tau_{rz} + b_z = \rho(r, z) \ddot{u}_z, \tag{12}$$

where  $b_i (i = r, z)$ ,  $\rho$  and  $u_i (i = r, z)$  are the body force, mass density and displacement, in  $r$  and  $z$  direction, respectively. Throughout the analysis, the dots over a quantity indicate the time derivative and a comma denotes the partial differentiation with respect to the spatial variables. According to solid mechanic's relations, for anisotropic and linear elastic materials, the constitutive equation in matrix form is:

$$\boldsymbol{\sigma} = \boldsymbol{\Delta}(\hat{r}) \boldsymbol{\varepsilon}, \tag{13}$$

In the above relation  $\boldsymbol{\sigma}$  and  $\boldsymbol{\varepsilon}$  are the matrix of stress and strain, respectively. For simplified equation it was proposed that:

$$(\hat{r}) = (r, z) . \tag{14}$$

$$\boldsymbol{\sigma} = [\sigma_{rr} \ \sigma_{\theta\theta} \ \sigma_{zz} \ \tau_{rz}]^T .$$

$$\boldsymbol{\varepsilon} = [\varepsilon_{rr} \ \varepsilon_{\theta\theta} \ \varepsilon_{zz} \ \gamma_{rz}]^T . \tag{15}$$

For an orthotropic cylinder, matrix  $\Delta(\hat{r})$  is presented as follows:

$$\Delta(\hat{r}) = \begin{bmatrix} \Delta_{11}(\hat{r}) & \Delta_{12}(\hat{r}) & \Delta_{13}(\hat{r}) & 0 \\ \Delta_{12}(\hat{r}) & \Delta_{22}(\hat{r}) & \Delta_{23}(\hat{r}) & 0 \\ \Delta_{13}(\hat{r}) & \Delta_{23}(\hat{r}) & \Delta_{33}(\hat{r}) & 0 \\ 0 & 0 & 0 & \Delta_{44}(\hat{r}) \end{bmatrix} , \tag{16}$$

where

$$\Delta_{11}(\hat{r}) = \frac{1 - \nu_{23}(\hat{r}) \nu_{32}(\hat{r})}{E_2(\hat{r}) E_3(\hat{r}) \beta} , \Delta_{22}(\hat{r}) = \frac{1 - \nu_{31}(\hat{r}) \nu_{13}(\hat{r})}{E_1(\hat{r}) E_3(\hat{r}) \beta} , \tag{17}$$

$$\Delta_{33}(\hat{r}) = \frac{1 - \nu_{21}(\hat{r}) \nu_{12}(\hat{r})}{E_1(\hat{r}) E_2(\hat{r}) \beta} ,$$

$$\Delta_{12}(\hat{r}) = \frac{\nu_{21}(\hat{r}) + \nu_{31}(\hat{r}) \nu_{23}(\hat{r})}{E_2(\hat{r}) E_3(\hat{r}) \beta} , \Delta_{23}(\hat{r}) = \frac{\nu_{32}(\hat{r}) + \nu_{12}(\hat{r}) \nu_{31}(\hat{r})}{E_1(\hat{r}) E_3(\hat{r}) \beta} , \tag{18}$$

$$\Delta_{13}(\hat{r}) = \frac{\nu_{31}(\hat{r}) + \nu_{21}(\hat{r}) \nu_{32}(\hat{r})}{E_2(\hat{r}) E_3(\hat{r}) \beta} , \Delta_{44}(\hat{r}) = G_{12}(\hat{r}) ,$$

$$\beta = \frac{1 - \nu_{32}(\hat{r}) \nu_{23}(\hat{r}) - \nu_{21}(\hat{r}) \nu_{12}(\hat{r}) - \nu_{13}(\hat{r}) \nu_{31}(\hat{r}) - 2\nu_{32}(\hat{r}) \nu_{21}(\hat{r}) \nu_{13}(\hat{r})}{E_1(\hat{r}) E_2(\hat{r}) E_3(\hat{r})} , \tag{19}$$

where  $\nu_{ij}$  ( $i, j = 1, 2, 3 \ i \neq j$ ),  $E_i$  ( $i = 1, 2, 3$ ) and  $G_{ij}$  ( $i, j = 1, 2, 3 \ i \neq j$ ) are Poisson's ratio , elasticity modulus and shear modulus, respectively.

In this study, it is assumed that the body force is zero, thus, we have

$$\sigma_{rr,r} + \tau_{rz,z} + \frac{1}{r} (\sigma_{rr} - \sigma_{\theta\theta}) = \rho(\hat{r}) \ddot{u}_r . \tag{20}$$

$$\tau_{rz,r} + \sigma_{zz,z} + \frac{1}{r} \tau_{rz} = \rho(\hat{r}) \ddot{u}_z . \tag{21}$$

The local weak-form of the governing equation (20) and (21) can be written as:

$$\int_{\Omega_q} \left\{ \sigma_{rr,r} + \tau_{rz,z} + \frac{1}{r} (\sigma_{rr} - \sigma_{\theta\theta}) - \rho(\hat{r}) \ddot{u}_r \right\} r W_r(\hat{r}) d\Omega = 0, \quad (22)$$

$$\int_{\Omega_q} \left\{ \tau_{rz,r} + \sigma_{zz,z} + \frac{1}{r} \tau_{rz} - \rho(\hat{r}) \ddot{u}_z \right\} r W_z(\hat{r}) d\Omega = 0, \quad (23)$$

where  $W_r(\hat{r})$  and  $W_z(\hat{r})$  are the weight or test functions.

$$\int_{\Omega_q} \sigma_{rr,r} W_r(\hat{r}) r d\Omega + \int_{\Omega_q} (\sigma_{rr} - \sigma_{\theta\theta}) W_r(\hat{r}) d\Omega + \int_{\Omega_q} \tau_{rz,z} W_r(\hat{r}) r d\Omega - \int_{\Omega_q} \rho(\hat{r}) \ddot{u}_r(\hat{r}, t) W_r(\hat{r}) r d\Omega = 0. \quad (24)$$

$$\int_{\Omega_q} \tau_{rz,r} W_z(\hat{r}) r d\Omega + \int_{\Omega_q} \sigma_{zz,z} W_z(\hat{r}) r d\Omega + \int_{\Omega_q} \tau_{rz} W_z(\hat{r}) d\Omega - \int_{\Omega_q} \rho(\hat{r}) \ddot{u}_z(\hat{r}, t) W_z(\hat{r}) r d\Omega = 0. \quad (25)$$

By applying the divergence theorem, equations (24) and (25) may be rewritten in the following form,

$$\int_{\Omega_q} (r W_{r,r}(\hat{r}) \sigma_{rr} + W_r(\hat{r}) \sigma_{\theta\theta} + r W_{r,z}(\hat{r}) \tau_{rz}) d\Omega - \int_{\Gamma_q} r W_r(\hat{r}) (n_r \sigma_{rr} + n_z \tau_{rz}) d\Gamma + \int_{\Omega_q} \rho(\hat{r}) \ddot{u}_r(\hat{r}, t) W_r(\hat{r}) r d\Omega = 0. \quad (26)$$

$$\int_{\Omega_q} (r \tau_{rz} W_{z,r}(\hat{r}) + r \sigma_{zz} W_{z,z}(\hat{r})) d\Omega - \int_{\Gamma_q} r W_z(\hat{r}) (n_r \tau_{rz} + n_z \sigma_{zz}) d\Gamma + \int_{\Omega_q} \rho(\hat{r}) \ddot{u}_z(\hat{r}, t) W_z(\hat{r}) r d\Omega = 0. \quad (27)$$

where  $\Omega_q$  is the domain of quadrature (local sub-domain) for node  $x$  (see Fig. 1) and  $\Gamma_q$  has composed by three parts, i.e.  $\Gamma_q = \Gamma_{qi} \cup \Gamma_{qu} \cup \Gamma_{qt}$ . The term  $\Gamma_{qi}$  is the internal boundary of the local sub-domain, which does not intersect with the global

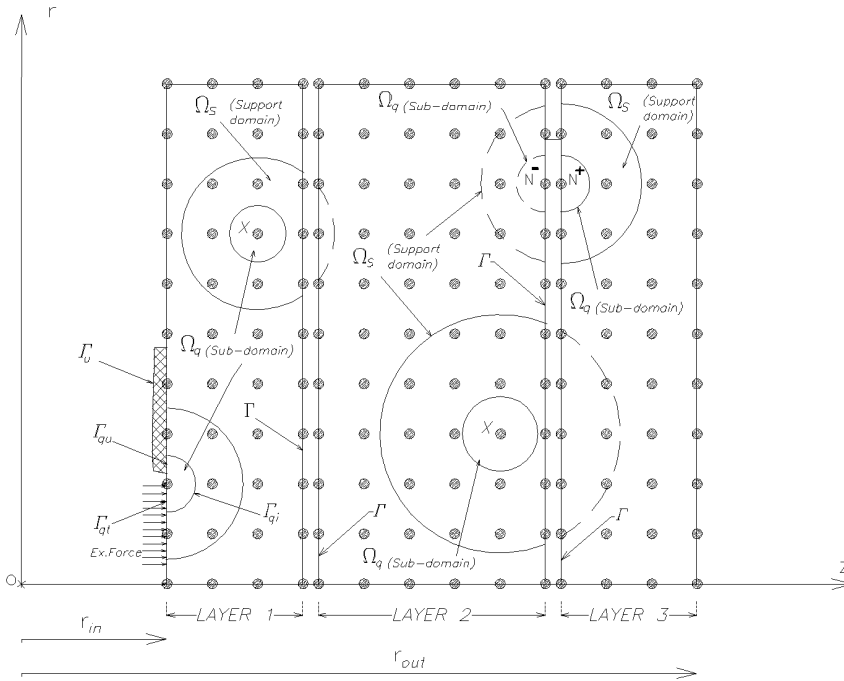


Figure 1: Local domains used in the MLPG method.

boundary  $\Gamma$ ;  $\Gamma_{qt}$  is the part of the natural boundary that intersects with the local sub-domain and  $\Gamma_{qu}$  is the part of the essential boundary that intersects with the local sub-domain.

Fig. 1 shows the employed local sub-domain and all kind of boundaries (natural boundary, internal boundary and essential boundary) in the MLPG method. Also in Fig. 1, the layers of cylinder and some sub-domains are shown in details. It can be seen, that the node  $X$  (as an interior node) lies in layer 2 but its support domain is located in both layers 2 and 3. It is assumed that the nodes within the support domain of node  $X$ , which are located in layer 3 do not influence on node  $X$ . The radius of sub-domain of interior nodes is assumed to be less than the minimum distances between nodes. As can be seen in Fig. 1, the nodes  $N^-$  and  $N^+$  locate on the interface of layers 2 and 3, respectively. It is assumed, that the support and sub-domains of node  $N^-$  lie on layer 2 and the support and sub-domains of node  $N^+$  lie on layer 3. Then, the continuity conditions between two nodes  $N^-$  and  $N^+$  should be satisfied.

The equations (26) and (27) can be taken into account in new form as follows:

$$\int_{\Omega_q} (r W_{r,r}(\hat{r}) \sigma_{rr} + W_r(\hat{r}) \sigma_{\theta\theta} + r W_{r,z}(\hat{r}) \tau_{rz}) d\Omega - \int_{\Gamma_{q_i} \cup \Gamma_{q_u}} r W_r(\hat{r}) (n_r \sigma_{rr} + n_z \tau_{rz}) d\Gamma + \int_{\Omega_q} \rho(\hat{r}) \ddot{u}_r(\hat{r}, t) W_r(\hat{r}) r d\Omega = \int_{\Gamma_{q_i}} r W_r(\hat{r}) (n_r \sigma_{rr} + n_z \tau_{rz}) d\Gamma . \tag{28}$$

$$\int_{\Omega_q} (r \tau_{rz} W_{z,r}(\hat{r}) + r \sigma_{zz} W_{z,z}(\hat{r})) d\Omega - \int_{\Gamma_{q_i} \cup \Gamma_{q_u}} r W_z(\hat{r}) (n_r \tau_{rz} + n_z \sigma_{zz}) d\Gamma + \int_{\Omega_q} \rho(\hat{r}) \ddot{u}_z(\hat{r}, t) W_z(\hat{r}) r d\Omega = \int_{\Gamma_{q_i}} r W_z(\hat{r}) (n_r \tau_{rz} + n_z \sigma_{zz}) d\Gamma . \tag{29}$$

The traction vector  $\mathbf{t}_i = \sigma_{ij} \mathbf{n}_j$ , ( $\mathbf{i}, \mathbf{j} = \mathbf{r}, \mathbf{z}$ ) is related to the stress vector, which leads to,

$$t_r = n_r \sigma_{rr} + n_z \tau_{rz} \tag{30}$$

$$t_z = n_z \sigma_{zz} + n_r \tau_{rz} \tag{31}$$

In the MLPG method, the global domain of the problem is divided to many sub-domains, in which a weak-form over the local sub-domains such as  $\Omega_q$  is constructed [Atluri (2004)]. These sub-domains can be overlapping each other, and cover the whole global domain (see Fig. 1). The local sub-domains could be of any geometric shape such as circle and rectangular with various sizes. In the present paper, the local sub-domains are taken to be a circular shape for simplicity. In such a case the calculation of domain-integrals is quite easy.

As shown in Fig. 1 the layered cylinder is discretized by the nodes located on the problem domain. The nodal variable is fictitious displacement component ( $r$ ) in the coordinate system. In the MLPG method, the trial function is chosen to be the interpolation over a number of nodes randomly distributed within the domain of influence. For the spatial distribution of function  $u$ , we apply the meshless approximation over a number of nodes randomly distributed within the domain of influence using the radial basis function (RBF). Thus, radial displacement variable can be expressed as:

$$\mathbf{u}^T(\hat{\mathbf{r}}, \mathbf{t}) = [u_r(\hat{r}, t) \quad u_z(\hat{r}, t)] ,$$

$$u_r(\hat{r}, t) = u_r(\bar{r}, t) = \sum_{i=1}^n R_i(\bar{r}) a_r^i = \mathbf{R}^T(\bar{\mathbf{r}}) \mathbf{a}_r(\mathbf{t}) , \quad \forall \bar{r} \in \Omega_s$$

$$u_z(\hat{r}, t) = u_z(\bar{r}, t) = \sum_{i=1}^n R_i(\bar{r}) a_z^i = \mathbf{R}^T(\bar{\mathbf{r}}) \mathbf{a}_z(\mathbf{t}) , \quad \forall \bar{r} \in \Omega_s \tag{32}$$

where  $a_k$  ( $k = r, z$ ) is the coefficient for the radial basis  $R_i(\bar{r})$  that is [Sladek, Sladek, Tanaka and Zhang (2005)]:

$$R_i(\bar{r}) = [\bar{r}^2 + c^2]^q, \tag{33}$$

$$\bar{r} = \left[ (r - r_i)^2 + (z - z_i)^2 \right]^{0.5}. \tag{34}$$

where the terms  $c$  and  $q$  are constant positive values. The values of  $q$  and  $c$  are selected equal to 0.5 and mean value of minimum distances between nodes, respectively. The number of radial basis functions  $n$  is determined by the number of nodes in the support domain. This form of shape function has been widely used in surface fitting and in constructing approximate solutions for partial differential equations. The vector  $\mathbf{R}$  has the following form,

$$\mathbf{R}^T(\bar{\mathbf{r}}) = [R_1(\bar{r}), R_2(\bar{r}), \dots, R_n(\bar{r})]. \tag{35}$$

which is the set of radial basis functions centered around  $r_i$ . The vectors  $\mathbf{a}_r$  and  $\mathbf{a}_z$  are defined as:

$$\mathbf{a}_r^T(\mathbf{t}) = [a_r^1(t), a_r^2(t), \dots, a_r^n(t)]. \tag{36}$$

$$\mathbf{a}_z^T(\mathbf{t}) = [a_z^1(t), a_z^2(t), \dots, a_z^n(t)].$$

From the interpolation equation (32) for the radial functions, the following system of linear equation for the coefficient  $\mathbf{a}$  is obtained as:

$$\mathbf{R}_0 \mathbf{a}(\mathbf{t}) = \hat{\mathbf{u}}(\mathbf{t}), \tag{37}$$

where

$$\hat{\mathbf{u}}_r^T = [u_r^1(t), u_r^2(t), \dots, u_r^n(t)],$$

$$\hat{\mathbf{u}}_z^T = [u_z^1(t), u_z^2(t), \dots, u_z^n(t)], \tag{38}$$

$$\hat{\mathbf{u}}^T(\mathbf{t}) = [\hat{u}_r \ \hat{u}_z],$$

It is composed of the time variable nodal values of displacements  $u_r^i(t)$  and  $u_z^i(t)$ , while  $\mathbf{R}_0$  is the matrix defined by nodal values of the RBFs as:

$$\mathbf{R}_0 = \begin{bmatrix} R_1(\bar{r}_1) & R_2(\bar{r}_1) & \dots & R_n(\bar{r}_1) \\ R_1(\bar{r}_2) & R_2(\bar{r}_2) & \dots & R_n(\bar{r}_2) \\ \dots & \dots & \dots & \dots \\ R_1(\bar{r}_n) & R_2(\bar{r}_n) & \dots & R_n(\bar{r}_n) \end{bmatrix}. \tag{39}$$

To calculate the vector  $\mathbf{a}(\mathbf{t})$ , we can write from equation (37),

$$\mathbf{a}(\mathbf{t}) = \mathbf{R}_0^{-1} \hat{\mathbf{u}}(\mathbf{t}). \tag{40}$$

The approximated function can be expressed in terms of the nodal values and the shape function as:

$$\mathbf{u}(\bar{\mathbf{r}}, \mathbf{t}) = \mathbf{R}^T(\bar{\mathbf{r}}) \mathbf{R}_0^{-1} \hat{\mathbf{u}}(\mathbf{t}) = \mathbf{\Phi}^T(\bar{\mathbf{r}}) \hat{\mathbf{u}}(\mathbf{t}), \quad (41)$$

Above equation can be rewritten in matrix form as:

$$\begin{bmatrix} u_r(\bar{r}, t) \\ u_z(\bar{r}, t) \end{bmatrix} = \sum_{i=1}^n \begin{bmatrix} \varphi^i(\bar{r}) & 0 \\ 0 & \varphi^i(\bar{r}) \end{bmatrix} \begin{bmatrix} u_r^i(t) \\ u_z^i(t) \end{bmatrix} = \sum_{i=1}^n \mathbf{\Phi}^i(\bar{\mathbf{r}}) \mathbf{u}^i(\mathbf{t}), \quad (42)$$

where  $\varphi^i(\bar{r})$  is the shape function associated with the node  $i$ . The nodal shape functions are presented as below:

$$\mathbf{\Phi}^T(\bar{\mathbf{r}}) = \mathbf{R}^T(\bar{\mathbf{r}}) \mathbf{R}_0^{-1}. \quad (43)$$

Matrix form of Eqs. 28 and 29 for  $I^{th}$  node can be found as:

$$\int_{\Omega_q} \mathbf{W}'_I \boldsymbol{\sigma} d\Omega - \int_{\Gamma_{qi} \cup \Gamma_{qu}} \mathbf{W}_I \mathbf{N}(\hat{\mathbf{r}}) \boldsymbol{\sigma} r d\Gamma + \int_{\Omega_q} \mathbf{W}_I \ddot{\mathbf{u}} \rho(\hat{r}) r d\Omega = \int_{\Gamma_{qt}} \mathbf{W}_I \mathbf{t} r d\Gamma, \quad (44)$$

where

$$\mathbf{W}' = \begin{bmatrix} rW_{r,r} & W_r & 0 & rW_{r,z} \\ 0 & 0 & rW_{z,z} & rW_{z,r} \end{bmatrix}. \quad (45)$$

According Hook's law in Eq. 13 the matrix of relation can be expressed as:

$$\boldsymbol{\sigma} = \boldsymbol{\Delta}(\hat{\mathbf{r}}) \sum_{i=1}^n \boldsymbol{\Psi}_i \mathbf{u}^i(\mathbf{t}), \quad (46)$$

and

$$\boldsymbol{\varepsilon} = \sum_{i=1}^n \boldsymbol{\Psi}_i \mathbf{u}^i(\mathbf{t}), \quad (47)$$

where the matrix  $\boldsymbol{\Psi}_i$  is represented by the gradients of the shape functions as:

$$\boldsymbol{\Psi}_i = \begin{bmatrix} \varphi_{,r}^i(\bar{r}) & 0 \\ \varphi^i(\bar{r})/r & 0 \\ 0 & \varphi_{,z}^i(\bar{r}) \\ \varphi_{,z}^i(\bar{r}) & \varphi_{,r}^i(\bar{r}) \end{bmatrix}. \quad (48)$$

The weight functions can be expressed in the matrix form as:

$$\mathbf{W} = \begin{bmatrix} W_r & 0 \\ 0 & W_z \end{bmatrix}. \quad (49)$$

The traction vector  $\mathbf{t}_i$  at a boundary point are approximated using the nodal values  $u^i(t)$  by:

$$\mathbf{t} = \mathbf{N}(\hat{\mathbf{r}}) \mathbf{\Delta}(\hat{\mathbf{r}}) \sum_{i=1}^n \mathbf{\Psi}_i \mathbf{u}^i(\mathbf{t}),$$

$$\mathbf{t} = \begin{bmatrix} t_r \\ t_z \end{bmatrix}.$$
(50)

where the matrix  $\mathbf{N}(\hat{\mathbf{r}})$  is related to the normal vector  $N(\hat{\mathbf{r}})$  on  $\Gamma_q$  by:

$$\mathbf{N}(\hat{\mathbf{r}}) = \begin{bmatrix} n_r & 0 & 0 & n_z \\ 0 & 0 & n_z & n_r \end{bmatrix}.$$
(51)

Substitution of equation (46) into (44) leads us to the following discrete systems of linear equations for the  $I^{th}$  node.

$$\int_{\Omega_q} \mathbf{W}'_I \mathbf{\Delta}(\hat{\mathbf{r}}) \sum_{i=1}^n \mathbf{\Psi}_i \mathbf{u}^i(\mathbf{t}) d\Omega - \int_{\Gamma_{qi} \cup \Gamma_{qu}} \mathbf{W}_I \mathbf{N}(\hat{\mathbf{r}}) \mathbf{\Delta}(\hat{\mathbf{r}}) \sum_{i=1}^n \mathbf{\Psi}_i \mathbf{u}^i(\mathbf{t}) r d\Gamma +$$

$$\int_{\Omega_q} \mathbf{W}_I \sum_{i=1}^n \mathbf{\Phi}^i(\bar{\mathbf{r}}) \ddot{\mathbf{u}}^i(\mathbf{t}) \rho(\hat{\mathbf{r}}) r d\Omega = \int_{\Gamma_{qt}} \mathbf{W}_I \mathbf{t} r d\Gamma,$$
(52)

Or

$$\sum_{i=1}^n \left\{ \int_{\Omega_q} \mathbf{W}'_I \mathbf{\Delta}(\hat{\mathbf{r}}) \mathbf{\Psi}_i d\Omega - \int_{\Gamma_{qi} \cup \Gamma_{qu}} \mathbf{W}_I \mathbf{N}(\hat{\mathbf{r}}) \mathbf{\Delta}(\hat{\mathbf{r}}) \mathbf{\Psi}_i r d\Gamma \right\} \mathbf{u}^i(\mathbf{t}) +$$

$$\sum_{i=1}^n \left\{ \int_{\Omega_q} \mathbf{W}_I \mathbf{\Phi}^i(\bar{\mathbf{r}}) \rho(\hat{\mathbf{r}}) r d\Omega \right\} \ddot{\mathbf{u}}^i(\mathbf{t}) = \int_{\Gamma_{qt}} \mathbf{W}_I \mathbf{t} r d\Gamma.$$
(53)

Equation (53) is transformed in the discretized system of ordinary differential equations, which may be written in the matrix form, as,

$$\mathbf{M}\ddot{\mathbf{u}} + \mathbf{K}\mathbf{u} = \mathbf{F}$$
(54)

where  $\mathbf{M}$ ,  $\mathbf{K}$  and  $\mathbf{F}$  are equivalent mass, stiffness and force matrix, respectively, which are described in the following:

$$\mathbf{M}_{ji} = \int_{\Omega_q} \mathbf{W}_I \mathbf{\Phi}^i(\bar{\mathbf{r}}) \rho(\hat{\mathbf{r}}) r d\Omega.$$
(55)

$$\mathbf{K}_{ji} = \int_{\Omega_q} \mathbf{W}'_I \Delta(\hat{\mathbf{r}}) \Psi_i d\Omega - \int_{\Gamma_{qi} \cup \Gamma_{qu}} \mathbf{W}_I \mathbf{N}(\hat{\mathbf{r}}) \Delta(\hat{\mathbf{r}}) \Psi_i r d\Gamma . \quad (56)$$

$$\mathbf{F} = \int_{\Gamma_{qt}} \mathbf{W}_I \mathbf{t} r d\Gamma . \quad (57)$$

In the MLPG method, the test and trial functions may be chosen from different functional spaces. In this study, test functions are chosen as the Heaviside unit step function with support on the local sub-domain, i.e.

$$W_r(\hat{\mathbf{r}}, t) = W_z(\hat{\mathbf{r}}, t) = \begin{cases} 1 & , \hat{\mathbf{r}} \in (\Omega_q \cup \Gamma_q) \\ 0 & , \hat{\mathbf{r}} \notin (\Omega_q \cup \Gamma_q) \end{cases} . \quad (58)$$

#### 4 Numerical results and discussions

In this section, numerical results are presented for a layered cylinder reinforced by FG carbon naotubes distributions subjected to shock loading. To verify the presented MLPG method, an infinite length layered cylinder reinforced by FG C-NTs distribution is assumed in which inner radius is  $r_i = 0.25 m$  and outer radius is  $r_o = 0.5m$ . The presented boundary conditions and material properties in ref. [Hosseini, Akhlaghi and Shakeri (2007)] are considered for the problem as follows.

$$\sigma_r(r_i, t) = P_i(t) . \quad (59)$$

$$\sigma_r(r_o, t) = 0 . \quad (60)$$

If the same boundary conditions with ref. [Hosseini, Akhlaghi and Shakeri (2007)] are assumed for the problem and also the terms  $V_{CN} = 0$  ,  $V_m = 0$  ,  $\eta_1 = \eta_2 = \eta_3 = 1$  are selected for the problem, it is possible to compare the obtained results with those reported in ref. [Hosseini, Akhlaghi and Shakeri (2007)].

It is assumed that

$$P_i(t) = \begin{cases} P_0 t & t \leq t_0 \\ 0 & t > t_0 \end{cases} , \quad (61)$$

where  $P_0 = 4 GPa/Sec$  and  $t_0 = 0.005 Sec$ . Fig. 2 shows a good agreement in comparison between results obtained by presented MLPG method and those reported in ref. [Hosseini, Akhlaghi and Shakeri (2007)].

As the second example, the following boundary conditions are assumed for the problem. In this simulation, a layered cylinder reinforced by FG carbon nanotubes distributions (FGCNTs) is considered to be made of three layers (see Figs. 1 and 3), which the inner and outer layers consist of Polymethyl-Methacrylate (PMMA) as matrix with CNTs as the fibers aligned in the radial or circumferential directions.

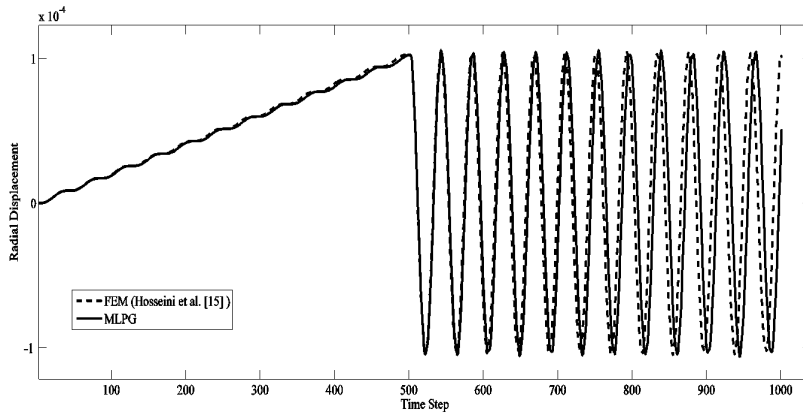


Figure 2: The comparison of obtained results from MLPG with those using FEM for radial displacement.

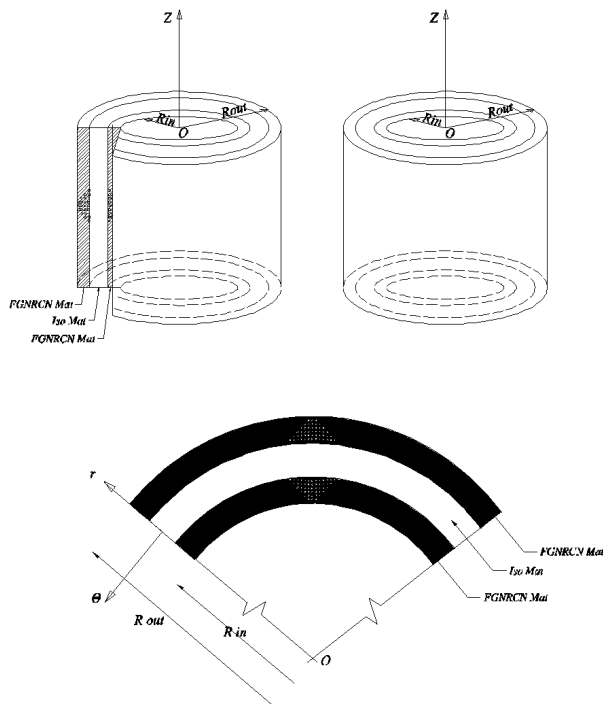


Figure 3: layered cylinder with three layers.

PMMA is an isotropic material with  $E^m = 2.5 \text{ GPa}$ ,  $\rho^m = 1150 \text{ kg/m}^3$  and  $\nu^m = 0.34$ .

The material properties applied for CNTs fibers are [Shen (2011)]:

$$E_1^{CN} = 5.6466 \text{ TPa}, E_2^{CN} = 7.0800 \text{ TPa}, G_{12}^{CN} = 1.9445 \text{ TPa}, \rho^{CN} = 1400 \text{ kg/m}^3 \text{ and } \nu_{12}^{CN} = 0.175.$$

Middle layer is isotropic material (Aluminum) with adopted property as below:

$$E_m = 70 \text{ GPa}, \rho_m = 2707 \text{ kg/m}^3, \nu_m = 0.3.$$

Geometry properties of this cylinder are shown in Table 1. The distributions of

Table 1: Geometry properties of the layered cylinder.

Position of layer	Thickness (cm)	$r_{min}$ (cm)	$r_{max}$ (cm)	Material type
Inner layer	20	50	70	FGCNTs Type UD,X,V, $\Delta$
Middle layer	40	70	110	Iso
Outer layer	20	110	130	FGCNTs Type UD,X,V, $\Delta$

modulus of elasticity for cylinder along the radial and circumferential directions are presented in Figs. 4 and 5, respectively.

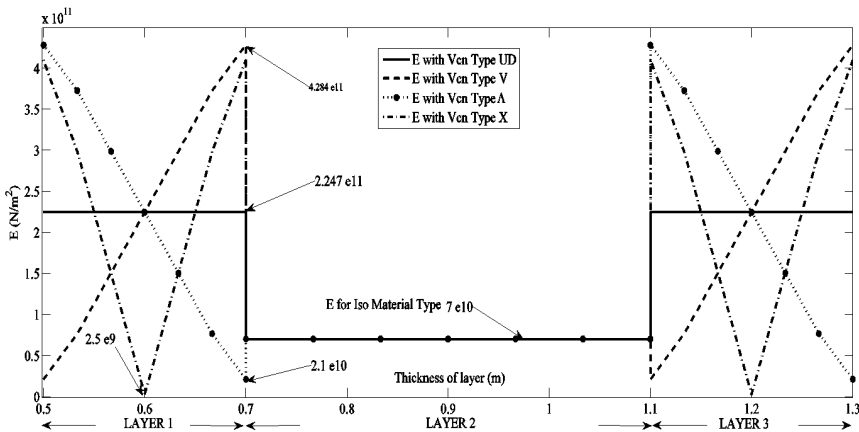


Figure 4: Variation of modulus of elasticity  $E_1$  along the CNTs as fibers for different Type of nanotube volume fraction.

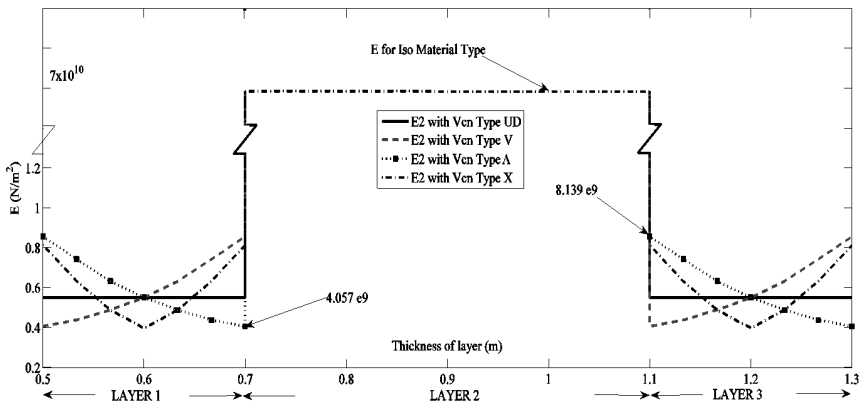


Figure 5: Variation of modulus of elasticity  $E_2$  perpendicular the CNTs as fibers for different Type of nanotube volume fraction.

The effects of various values of  $V_{CN}^*$  on time histories of radial displacement can be found in Figs. 6 to 9 for four distributions of carbon nanotubes, which are plotted for point located at middle of the layered cylinder when fiber direction of CNTs is located in  $r$  direction.

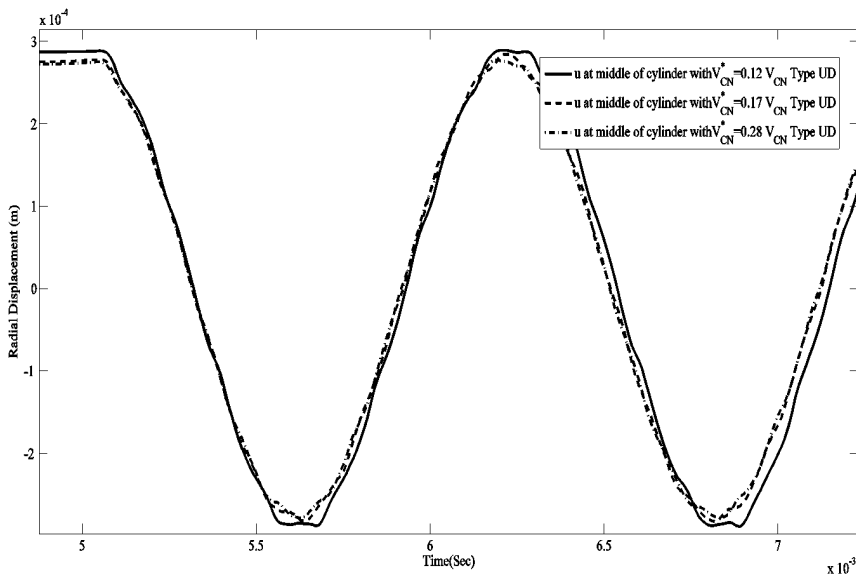


Figure 6: Time history of radial displacement of a certain point for various values of  $V_{CN}^*$  and uniform distribution of CNTs.

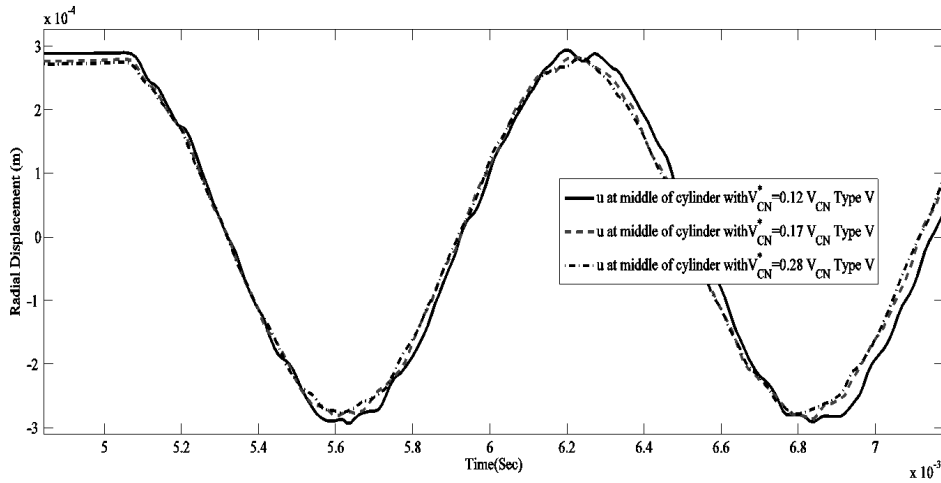


Figure 7: Time history of radial displacement of a certain point for various values of  $V_{CN}^*$  and FG Type V of CNTs.

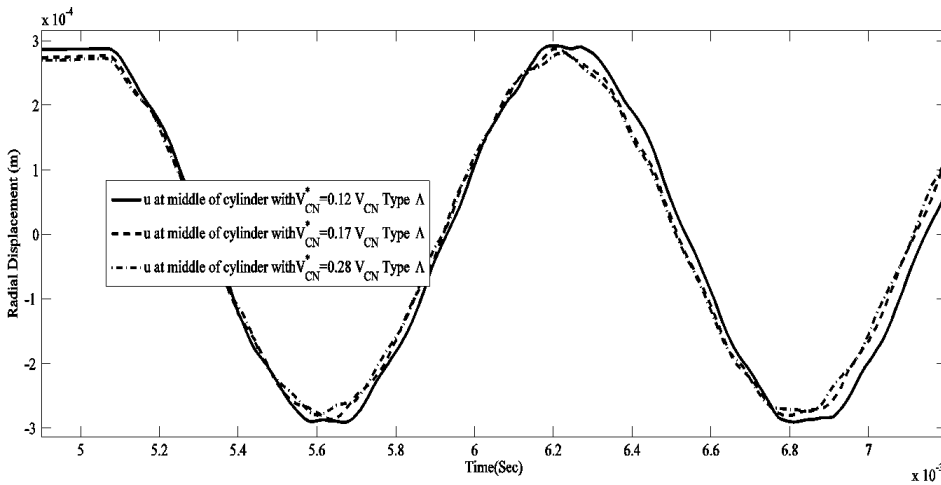


Figure 8: Time history of radial displacement of a certain point for various values of  $V_{CN}^*$  and FG Type  $\Lambda$  of CNTs.

It is concluded from Figs. 6 to 9 that the amplitude of variation in time domain is decreased when the value of  $V_{CN}^*$  is increased. Also, the differences between time histories of displacement for various volume fractions of CNTs are negligible and

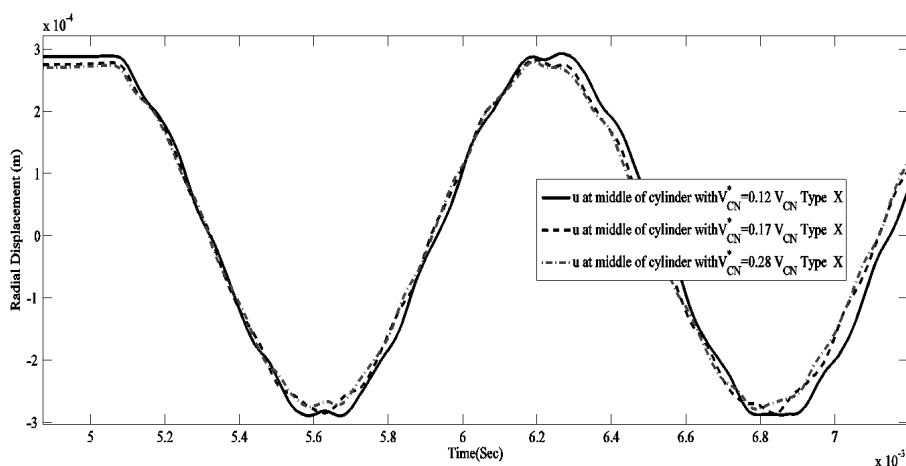


Figure 9: Time history of radial displacement of a certain point for various values of  $V_{CN}^*$  and FG Type X of CNTs.

very low. It is concluded that the CNTs fibers, which are aligned through radius direction, have small effect on time history of displacement.

The effects of  $V_{CN}^*$  on time histories of radial displacement are shown in Figs 10 to 13, in which the fiber directions are aligned along  $\theta$  direction. The amplitude of variation in time domain decreased when the value of  $V_{CN}^*$  increased.

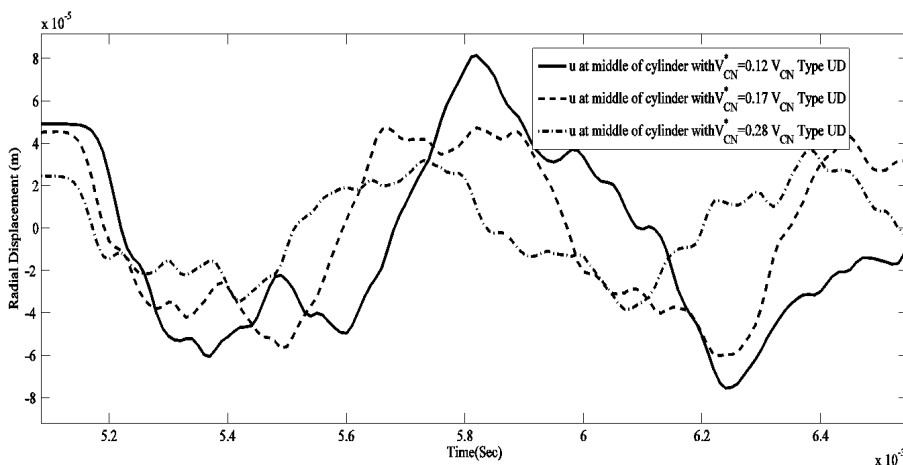


Figure 10: Time history of radial displacement of a certain point for various values of  $V_{CN}^*$  and uniform distribution of CNTs.

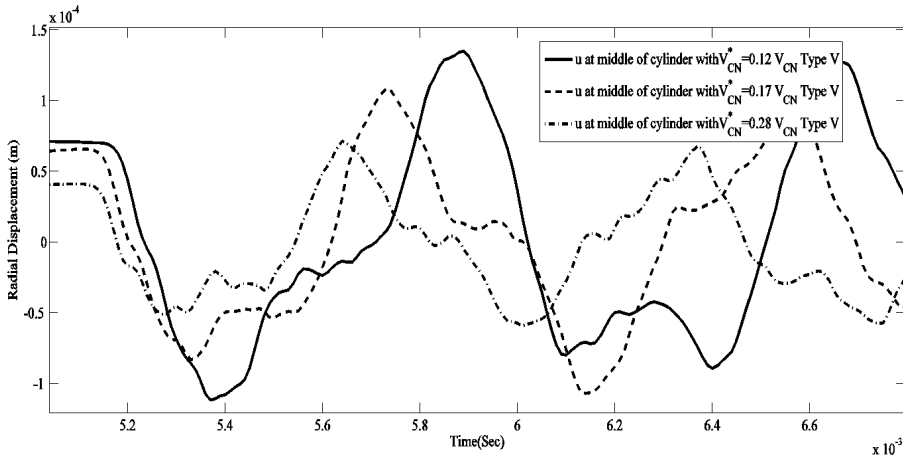


Figure 11: Time history of radial displacement of a certain point for various values of  $V_{CN}^*$  and FG Type V of CNTs.

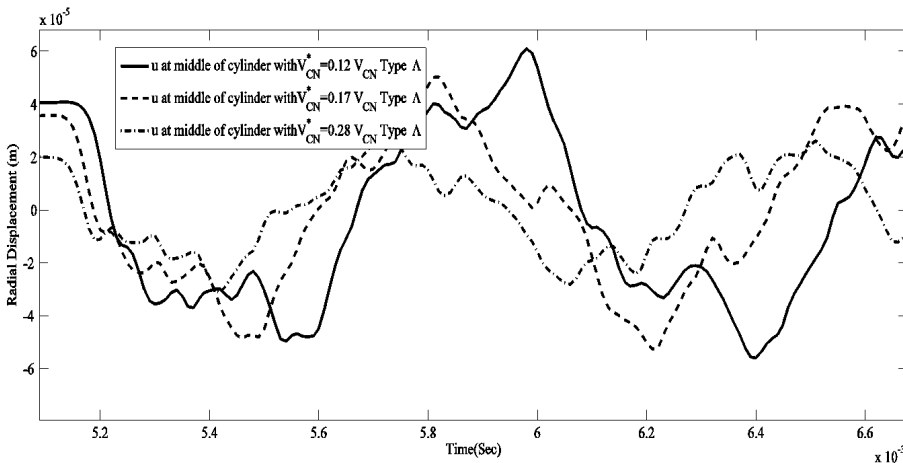


Figure 12: Time history of radial displacement of a certain point for various values of  $V_{CN}^*$  and FG Type A of CNTs.

As shown in Figs. 10 to 13, there are significant differences between time histories of displacement that are obtained for various volume fractions of CNTs. It is concluded that the CNTs fibers, which are aligned through circumferential direction, have a high influence on time history of displacement. Effect of volume fraction of carbon nanotubes on the maximum displacement of layered cylinder is shown in Table 2.

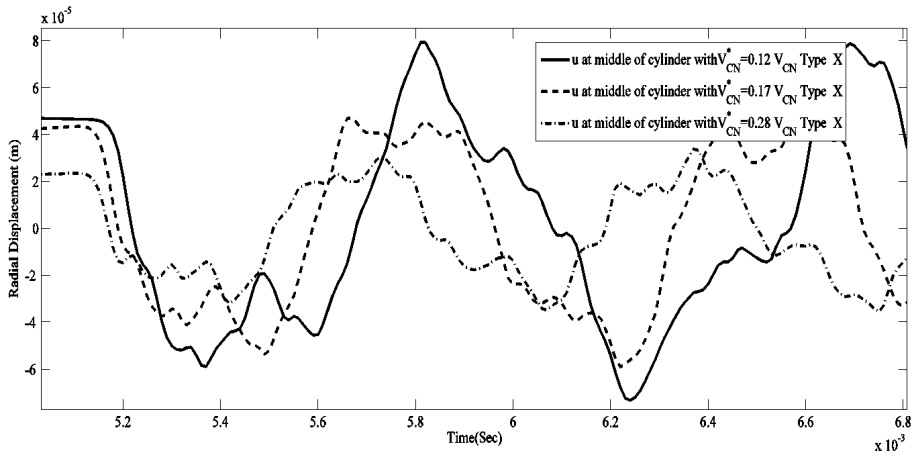


Figure 13: Time history of radial displacement of a certain point for various values of  $V_{CN}^*$  and FG Type X of CNTs.

Table 2: Effect of volume fraction and direction of CNTs on maximum displacement.

FGCNTs Type	$V_{CN}^*$	Max displacement; CNTs aligned in r direction (m)	Max displacement; CNTs aligned in $\theta$ direction (m)
CNTs Type UD	0.12	$3.8918 e - 4$	$6.4254 e - 4$
CNTs Type V	0.12	$4.3725 e - 4$	$9.5642 e - 4$
CNTs Type $\Lambda$	0.12	$4.1955 e - 4$	$4.8775 e - 4$
CNTs Type X	0.12	$4.2308 e - 4$	$5.5298 e - 4$
CNTs Type UD	0.17	$3.6442 e - 4$	$4.1526 e - 4$
CNTs Type V	0.17	$4.0136 e - 4$	$6.1894 e - 4$
CNTs Type $\Lambda$	0.17	$3.8643 e - 4$	$3.0898 e - 4$
CNTs Type X	0.17	$3.8905 e - 4$	$3.5837 e - 4$
CNTs Type UD	0.28	$3.5111 e - 4$	$3.0406 e - 4$
CNTs Type V	0.28	$3.7453 e - 4$	$5.0966 e - 4$
CNTs Type $\Lambda$	0.28	$3.6390 e - 4$	$2.0790 e - 4$
CNTs Type X	0.28	$3.6542 e - 4$	$2.4631 e - 4$

As shown in Table 2, FGCNTs type  $\Lambda$  is more effective on reduce of maximum displacement comparing to other types.

It is concluded from Table 2 that the maximum displacement decreases when the value of  $V_{CN}^*$  is increased. The orientation of CNT fiber through  $\theta$  direction has more influence on dynamic behavior of displacement comparing to orientation through radial direction. By considering a fixed value for “ $V_{CN}^*$ ” as “ $V_{CN}^* = 0.12$ ” and “ $V_{CN}^* = 0.28$ ”, the time histories of radial displacement of middle point on thickness for fiber CNTs aligned  $\theta$  direction are shown for various type of FGCNTs in Figs. 14 and 15.

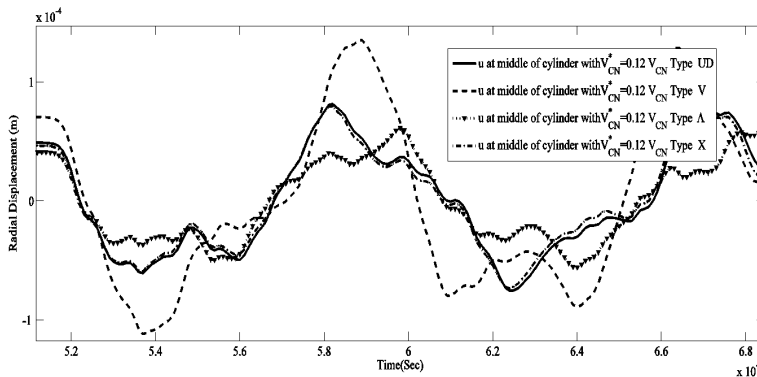


Figure 14: Time history of radial displacement for middle point on thickness of cylinder for certain value of  $V_{CN}^* = 0.12$ .

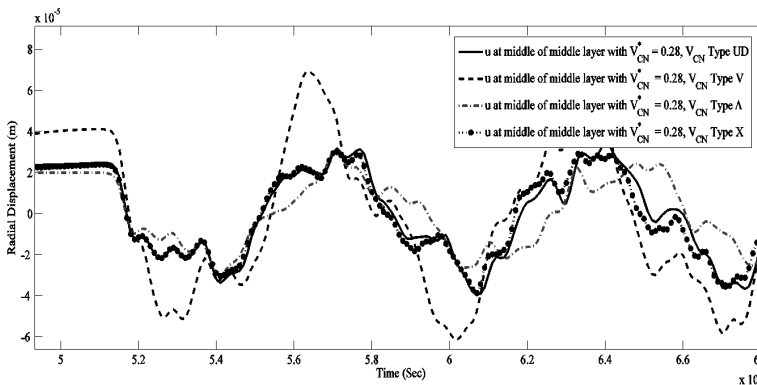


Figure 15: Time history of radial displacement for middle point on thickness of cylinder for certain value of  $V_{CN}^* = 0.28$ .

It is evident in Figs. 14 and 15 that the amplitude of displacement variation decreases by increasing the value of  $V_{CN}^*$ .

The time histories of radial displacement of middle point on thickness of each layer for layered cylinder reinforced by FG carbon naotubes distributions type  $\Lambda$  with  $V_{CN}^* = 0.12$  and  $V_{CN}^* = 0.28$  are illustrated in Figs. 16 and 17. It can be seen that by increasing the value of radius, the values of peak points are decreased and the frequency of variation is increased.

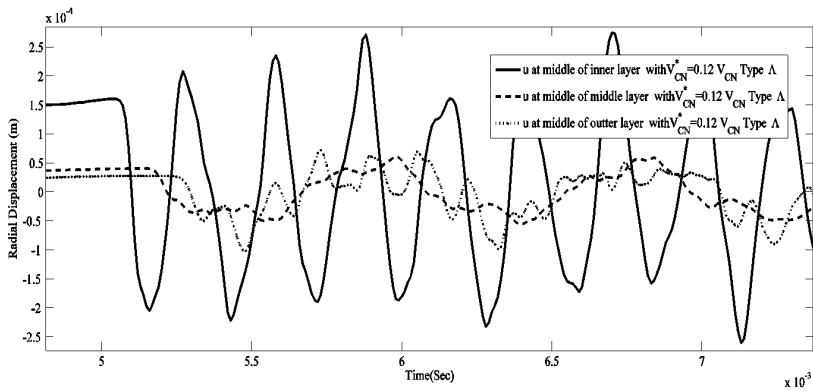


Figure 16: Time history of radial displacement for middle point on thickness of each layer for certain value of  $V_{CN}^* = 0.12$ .

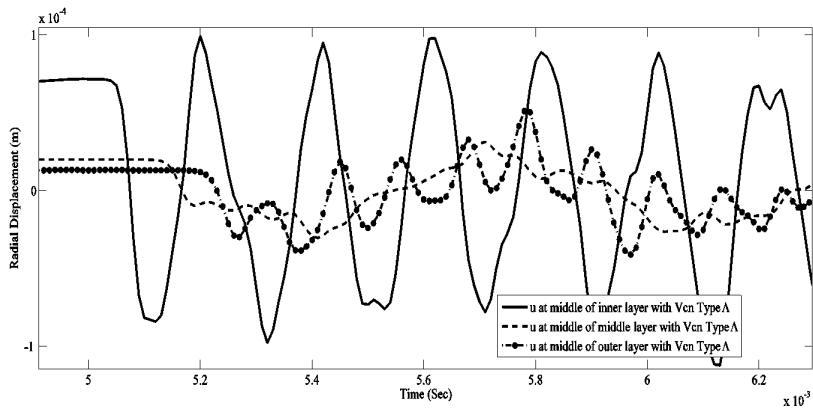


Figure 17: Time history of radial displacement for middle point on thickness of each layer for certain value of  $V_{CN}^* = 0.28$ .

## 5 Conclusions

In this study, a meshless technique based on meshless local Petrov – Galerkin (MLPG) method is developed for dynamic analysis of a layered cylinder reinforced by functionally graded carbon nanotubes distributions. The axisymmetry conditions are assumed for the problem and volume fraction of CNTs distributions is supposed to vary continuously along thickness direction at each inner and outer layer. To obtain the dynamic behavior of displacement in time domain, the meshless local Petrov-Galerkin (MLPG) method is combined with Newmark finite difference method. A unite step function is used as the test function in the local symmetric weak-form. The layered cylinder consists of three layers so that each layer has its support domain and distinct property. Nodes at each layer do not influence nodes lie at other layers and only affect nodes at its layer which is located on its support domain.

The analyzed domain at each layer is divided into small circular sub-domains on which the local integral equation is derived. The radial basis functions are adopted for approximation of field variables. The major conclusions resulting from the above analysis can be summarized as follows:

- The wave motion in the reinforced layered cylinder is formulated based on meshless local Petrov-Galerkin (MLPG) method for elastic wave propagation analysis.
- It is possible that the time histories of displacement are assessed for various grading patterns on CNTs distributions in some points on the body of cylinder by using the presented meshless technique.
- The accuracy and the convergence of the presented method for plane strain wave propagation analysis in a cylinder have been tested under time dependent boundary conditions as shock loading.
- The presented method can be extended to study 2D and 3D elastic wave propagation in a layered cylinder reinforced by functionally graded carbon nanotubes distributions with various transient boundary conditions.
- The type  $\Lambda$  of CNTs distributions has smaller displacements comparing with the other types.
- By increasing the nanotube volume fraction  $V_{CN}^*$ , the value of radial displacements are decreased.

- By comparing the aligned fibers through  $r$  direction with the aligned fibers through  $\theta$  direction, it can be concluded the aligned fibers through  $\theta$  direction are more effective to decrease the maximum values of displacements.

## References

- Atluri, S. N.** (2004): *The Meshless Method (MLPG) for Domain and BIE Discretizations*. Tech Science Press, Encino.
- Atluri, S. N.; Shen, S.** (2002): The Meshless Local Petrov-Galerkin (MLPG) Method: A Simple & Less-costly Alternative to the Finite Element and Boundary Element Methods. *CMES: Computer Modeling in Engineering and Sciences*, vol. 3, no. 1, pp. 11-51.
- Atluri, S. N.; Zhu, T.** (1998): A new meshless local Petrov-Galerkin (MLPG) approach in computational mechanics. *Computational Mechanics*, vol. 22, pp. 117-127.
- Awaji, H.** (2001): Temperature and stress distributions in a plate of functionally graded materials. *Fourth International Congress on thermal stresses*, June 8-11, 2001, Osaka, Japan.
- Benbouza, N.; Louai, F. Z.; Nait-Said, N.** (2008): Application of Meshless Petrov-Galerkin (MLPG) method in electromagnetic using Radial Basis Functions. *Power Electronics, Machines and Drives*, 2008. PEMD 2008.4th IET Conference on Publication, pp. 650 – 655.
- Bert, C. W.; Baker, J. L.; Egle, D. M.** (1969): Free vibration of multilayer anisotropic cylindrical shells. *Journal of Computational Mathematics*, vol. 3, p-p. 480-499.
- Coto, B.; Antia, I.; Blanco, M.; Martinez-de-Arenaza, I.; Meaurio, E.; Barriaga, J.; Sarasua, J. R.** (2011): Molecular dynamics study of the influence of functionalization on the elastic properties of single and multiwall carbon nanotubes. *Computational Materials Science*, vol. 50, pp. 3417-3424.
- Dong, S. B.** (1968): Free vibration of laminated orthotropic cylindrical shells. *Journal of the Acoustical Society of America*, vol. 44, pp. 1628-1635.
- El-abbasi, N.; Meguid, S. A.** (2000): Finite element modeling of the thermoelastic behavior of functionally graded plates and shells. *International Journal of Computational Engineering Science*, vol. 1, no. 1, pp. 151-165.
- Fukui, Y.; Yamanaka, N.** (1992): Elastic analysis for thick-walled tubes of functionally graded material subjected to internal pressure. *The Japan Society of Mechanical Engineers International Journal Series I*, vol. 35, no. 4, pp. 379-385.
- Ghayumizadeh, H.; Shahabian, F.; Hosseini, S. M.** (2013): Elastic wave prop-

agation in a functionally graded nanocomposite reinforced by carbon nanotubes employing meshless local integral equations (LIEs). *Engineering Analysis with Boundary Element Method*, vol. 37, pp. 1524-1531.

**Greenberg, J. B.; Stavsky, Y.** (1980): Buckling and vibration of orthotropic composite cylindrical shells. *Acta Mechanica*, vol. 36, pp. 15-29.

**Gu, Y. T.; Liu, G.R.** (2001): A Meshless Local Petrov-Galerkin (MLPG) method for free and forced vibration analyses for solids. *Computational Mechanics*, vol. 27, pp. 188-198.

**Han, Y.; Elliott, J.** (2007): Molecular dynamics simulations of the elastic properties of polymer/carbon nanotube composites. *Computational Materials Science*, vol. 39, pp. 315-323.

**Hosseini, S. M.** (2013): Natural frequency analysis in functionally graded nanocomposite cylinders reinforced by carbon nanotubes using a hybrid mesh-free method. *CMES: Computer Modeling in Engineering and sciences*, vol. 95, no. 1 pp. 1-29.

**Hosseini, S. M.; Akhlaghi, M.; Shakeri M.** (2007): Dynamic Response and Radial Wave Propagation Velocity in Thick Hollow Cylinders Made of Functionally Graded Materials. *Engineering Computations*, vol. 24, pp. 288-303.

**Hosseini, S. M.; Shahabian, F.; Sladek, J.; Sladek, V.** (2011): Stochastic meshless local Petrov-Galerkin (MLPG) method for thermo-elastic wave propagation analysis in functionally graded thick hollow cylinders. *CMES: Computer Modeling in Engineering and Sciences*, vol. 71, no. 1, pp. 39-66.

**Hosseini, S. M.; Sladek, J.; Sladek, V.** (2011): Meshless local Petrov-Galerkin method for coupled thermoelasticity analysis of a functionally graded thick hollow cylinder. *Engineering Analysis with Boundary Element*, vol. 35, no. 6, pp. 827-835

**Jabbari, M.; Sohrabpour, S.; Eslami M. R.** (2002): Mechanical and thermal stresses in a functionally graded hollow cylinder due to radially symmetric loads. *International Journal of Pressure Vessels and Piping*, vol. 79, pp. 493-497.

**Loy, C. T.; Lam, K. Y.; Reddy, J. N.** (1999): Vibration of functionally graded cylindrical shells. *International Journal of Mechanical Sciences*, vol. 41, pp. 309-324.

**Lei, Z. X.; Liew, K. M.; Yu, J. L.** (2013a): Buckling analysis of functionally graded carbon nanotube-reinforced composite plates using the element-free kp-Ritz method. *Composite Structures*, vol. 98, pp. 160-168.

**Lei, Z. X.; Liew, K. M.; Yu, J. L.** (2013b): Large deflection analysis of functionally graded carbon nanotube-reinforced composite plates by the element-free kp-Ritz method. *Computer Methods in Applied Mechanics and Engineering*, vol. 256, pp.

189–199.

**Moradi-Dastjerdi, R.; Foroutan, M.; Pourasghar, A.** (2013): Dynamic analysis of functionally graded nanocomposite cylinders reinforced by carbon nanotube by a mesh-free method. *Materials & Design*, vol. 44, pp. 256-266.

**Praveen, G. N.; Reddy J. N.** (1998): Nonlinear transient thermoelastic analysis of functionally graded ceramic-metal plates. *International Journal of Solids and Structures*, vol. 35, pp. 4457–4476.

**Shahsiah, R.; Eslami, M. R.** (2003): Functionally graded cylindrical shell thermal instability based on improved Donnell equations. *AIAA J*, vol. 41, no. 9, pp. 1819-1826.

**Shen, H. S.** (2009): Nonlinear bending of functionally graded carbon nanotube reinforced composite plates in thermal environments. *Composite Structures*, vol. 91, pp. 9–19.

**Shen, H. S.** (2011): Postbuckling of nanotube–reinforced composite cylindrical shells in thermal environments, Part I: axially-loaded shells. *Composite Structures*, vol. 93, pp. 2096–2108.

**Sladek, J.; Sladek, V.; Zhang, C.** (2003): Application of meshless local Petrov-Galerkin (MLPG) method to elastodynamic problems in continuously nonhomogeneous solids. *CMES: Computer Modeling in Engineering and Sciences*, vol. 4, no. 6, pp. 637–647.

**Sladek, V.; Sladek, J.; Tanaka, M.; Zhang, C.** (2005): Transient heat conduction in anisotropic and functionally graded media by local integral equations. *Engineering Analysis with Boundary Element Method*, vol. 29, pp. 1047–1065.

**Soares, J. D.; Sladek, J.; Sladek, V.** (2009): Dynamic analysis by meshless local Petrov-Galerkin formulations considering a time-marching scheme based on implicit green's functions. *CMES: Computer Modeling in Engineering and Sciences*, vol. 50, no. 2, pp. 115–140.

**Soares, J. D.; Sladek, J.; Sladek, V.** (2010): Non-linear dynamic analyses by meshless local Petrov-Galerkin formulations. *International Journal for Numerical Methods in Engineering*, vol. 81, pp. 1687–1699.

**Stavsky, Y.; Loewy, R.** (1971): On vibrations of heterogeneous orthotropic cylindrical shells. *Journal of Sound and Vibration*, vol. 15, pp. 235-256.

**Yamada, G.; Irie, T. M.; Tsushima.** (1984): Vibration and stability of orthotropic circular cylindrical shells subjected to axial load. *Journal of the Acoustical Society of America*, vol. 75, pp. 842-848.

**Zimmerman, R. W.; Lutz, M. P.** (1999): Thermal stress and thermal expansion in a uniformly heated functionally graded cylinder. *Journal of Thermal Stresses*, vol.

22, pp. 88–177.

**Zhu, R.; Pan, E.; Roy A. K.** (2007): Molecular dynamics study of the stress-strain behavior of carbon-nanotube reinforced Epon 862 composites. *Materials Science and Engineering: A*, vol. 447, pp. 51-57.

